catalysts

MDPI

Article

A Bifunctional Electroactive Ti_4O_7-Based Membrane System for Highly Efficient Ammonia Decontamination

Wenchang Zhao [1], Jiancheng Mei [2], Yanbiao Liu [2,3,*], Bo Yang [2], Fang Li [2,3], Xiaofeng Fang [2], Manhong Huang [2,3] and Wolfgang Sand [2,4]

1 College of Chemistry and Materials, Ningde Normal University, Ningde, Fujian 352100, China; wenchangzhao@foxmail.com

2 Textile Pollution Controlling Engineering Center of Ministry of Environmental Protection, College of Environmental Science and Engineering, Donghua University, 2999 North Renmin Road, Shanghai 201620, China; 2181540@mail.dhu.edu.cn (J.M.); yangbo@dhu.edu.cn (B.Y.); lifang@dhu.edu.cn (F.L.); fxf595@dhu.edu.cn (X.F.); huangmanhong@dhu.edu.cn (M.H.); wolfgang.sand@uni-due.de (W.S.)

3 Shanghai Institute of Pollution Control and Ecological Security, 1239 Siping Road, Shanghai 200092, China

4 Institute of Biosciences, Freiberg University of Mining and Technology, 09599 Freiberg, Germany

* Correspondence: yanbiaoliu@dhu.edu.cn; Tel.: +86-021-67798752

Received: 11 March 2020; Accepted: 30 March 2020; Published: 1 April 2020

Abstract: Herein, an electroactive filtration system, consisting of a Ti_4O_7 anode and a Pd-Cu co-modified nickel foam cathode, was developed and applied for the decontamination of ammonia from water. When assisted with an external electrical field, ClO• was generated on the surface of the Ti_4O_7 anode, which then reacted selectively with ammonia to generate N_2. The anodic byproduct, NO_3^-, could also be reduced efficiently at the functional cathode to produce N_2 as well. Electron paramagnetic resonance technique and radical scavenging tests synergistically verified the essential role of ClO• during the highly efficient ammonia conversion process. Relative to conventional batch systems, the developed flow-through design demonstrated enhanced ammonia conversion kinetics, thanks to the convection-enhanced mass transport. The proposed technology also showed desirable stability across a wide environmental matrix. This work provides new insights for the development of advanced and affordable continuous-flow systems towards effective decontamination of ammonia.

Keywords: Ti_4O_7; ammonia decontamination; ClO•; flow-through

1. Introduction

Excessive ammonia in the water environment usually causes eutrophication of water bodies and poses toxic effect to aquatic organisms [1,2]. Therefore, reducing the ammonia emission has been one of the primary objectives of current wastewater treatment processes. Among these available remediation processes, electrochemical oxidation was considered as a promising approach, due to its environmental friendliness, high efficiency, and easy controllability. The electrochemical processes have demonstrated enhanced oxidation power for the degradation of various toxic and refractory organic contaminants. For example, a Bi-doped SnO_2/Ti_4O_7 composite electrode was proven to be effective for the complete mineralization of atrazine and clothianidin within a few seconds at an applied potential of 3.5 V vs. SHE [3]. In an electrochemical system, both the electrode materials and reactor configuration play essential roles in determining the overall system performance (Table S1).

In terms of the electrode materials, several advanced types have been reported, such as boron-doped diamond (BDD), doped SnO_2, and carbon nanotubes (CNT) [4]. The BDD electrode possesses a wide potential window and high anodic stability, but suffers from high manufacturing cost [5]. The doped SnO_2 electrode demonstrated good performance and acceptable cost, but with limited service life [6]. While the CNT electrode possesses superior conductivity and a high specific surface area, the potential release of nanoscale CNT powders may cause secondary pollution [7]. Alternatively, sub-stoichiometric titanium oxide materials have attracted much recent interest from the scientific community for electrocatalytic applications due to their high conductivity, low cost, strong corrosion resistance, and excellent stability [8]. Among the family of sub-stoichiometric titanium oxide materials, Ti_4O_7 exhibits the highest conductivity, up to 1500 S cm^{-1}, and excellent resistance to harsh chemical conditions [3,9].

Regarding the reactor design, traditional electrochemical processes usually adopt flat plate electrodes and operate in flow-by mode. However, such a flow configuration usually leads to a large hydrodynamic diffuse boundary layer of > 100 μm [10]. Extensive experimental studies and modeling data suggest that an oxidation reaction only happens within a narrow zone of < 1 μm at the electrode/solution interface [11]. To address this issue, an effective solution, combining electrochemical oxidation with membrane filtration, was proposed, which can be operated in an alternative flow-through configuration. Convection flow perpendicular to the "active" membrane improves the mass transport of reactants towards the active sites by restricting the diffusive distance to the pore radius of the membrane electrode. For example, Zaky and Chaplin previously reported that a Ti_4O_7-based electroactive membrane showed a 10-fold increase in mass transport rate when compared with that obtained in traditional flow-by mode [8]. Meanwhile, such flow-through design is attractive for practical engineering applications, due to its simple controllability and high operability. However, there are only very limited reports available on the decontamination of ammonia from water bodies using a flow-through system. It can be envisaged that by adopting a flow-through design with high-performance electrode materials, rapid and effective ammonia nitrogen removal would be achieved.

We have previously developed a flow-by Ti_4O_7–based electrochemical system that enables ammonia conversion under an electric field [12]. However, the poor mass transport in that design significantly limits the potential for large-scale application of this promising technology. Herein, we further developed a flow-through system using the Ti_4O_7 electrode as a functional anode, as well as a membrane material. When assisted by an external electric field, we hypothesized that the flow-through Ti_4O_7 electrode enables consistent production of highly reactive OH•, which further reacts with free chlorine to generate ClO•; these ClO• can react quickly with electron-rich groups to selectively convert ammonia to N_2 [13]. Meanwhile, a Pd-Cu co-modified nickel foam (Pd-Cu/NF) cathode enables the reduction of anodic byproduct—nitrate—to N_2 again. At both electrodes, the dominant product is N_2. The influence of several key operating factors (e.g., anode potential, Cl^- concentration, and solution pH) on the ammonia decontamination performance were systematically investigated. The electron paramagnetic resonance (EPR) technique and scavenger experiments both confirmed the essential role of ClO• within the proposed system. This work is dedicated to providing an effective and affordable design for the decontamination of aqueous pollutants, based on the promising sub-stoichiometric titanium oxide materials.

2. Results and Discussion

2.1. Characterizations

The morphology of Ti_4O_7 electrodes was characterized by field emission scanning electron microscopy (FESEM). Figure S1a reveals that the macroscale Ti_4O_7 particles were interconnected and formed macroporous structure. This led to a BET surface area of 2.8 ± 0.4 m^2 g^{-1} for the Ti_4O_7 anode [14]. X-ray diffraction (XRD) patterns of the electrode materials, in accordance with that of standard spectra

of Ti_4O_7, with characteristic peaks centered at 20.8°, 26.2°, 29.5°, 31.6°, 34.0°, 36.2°, 40.5°, 53.1°, 55.0°, 63.7°, and 66.3° (indicated by red points) (Figure S1b). Other Magnéli phases were not observed in the XRD pattern, indicating a high-purity Magnéli phase Ti_4O_7 electrode has been successfully prepared during the high-temperature fabrication process. The presence of Magnéli phase Ti_4O_7 as the main component ensures an excellent electrical conductivity because Ti_4O_7 exhibits excellent conductivity, compared with other sub-stoichiometric titanium oxides [15]. The X-ray photoelectron spectroscopy (XPS) survey pattern of the Ti_4O_7 electrode confirms the presence of C 1s, O 1s, and Ti 2p with specific ratio of 21.91, 54.92, and 23.17%, respectively. The Ti 2p characteristic peaks centered at 458.7 eV ($2p_{3/2}$) and 464.3 eV ($2p_{1/2}$) can be assigned to Ti^{4+}, while peaks located at 456.2 eV ($2p_{3/2}$) and 461.9 eV ($2p_{1/2}$) can be assigned to Ti^{3+} (Figure S1d) [16,17]. As displayed in Figure S2, the C 1s XPS spectra can be divided into three peaks centered at 284.5 eV, 285.9 eV, and 288.3 eV, corresponding to C=C, C–O, and C=O, respectively. While the high resolution O 1s spectrum were deconvoluted into two peaks centered at 529.7 eV and 531.1 eV, respectively, corresponding to Ti–O bond and –OH group [18].

Compared to original gray NF, the color of the Pd-Cu/NF changed to black after the loading of Cu and Pd (Figure S3), although the macropore size and surface morphology did not change significantly (Figure S4) [6]. Such macroporous dimensions of the Pd-Cu/NF cathode only generated a BET surface area of 1.3 ± 0.1 $m^2\ g^{-1}$. The presence of Pd and Cu in NF can also be verified by the XPS technique, as well. The bonding energy of the spin-orbit coupling of metal Pd^0 can be observed at 340.5 eV and 335.2 eV, respectively. Another pair of Pd^{2+} signals were observed at 342.2 eV and 337.0 eV (Figure S4c). The successful deposition of Cu onto the NF can be verified by the Cu 2p XPS spectra. As displayed in Figure S4d, the signals located at 931.8 eV and 953.0 eV were assignable to the emissions from Cu 2p 3/2 and Cu2p 1/2 levels, which corresponded to the typical binding energy of Cu^0 [19]. Other binding energies present at 934.4 eV for Cu $2p_{3/2}$ and 954.0 eV for Cu $2p_{1/2}$ were ascribed to Cu^{2+} [6,20]. Besides these peaks, the presence of shake-up satellite peaks within the region of 940–945 eV (Cu $2p_{3/2}$) and 959–965 eV (Cu $2p_{1/2}$) also indicated the presence of Cu^{2+} species on the cathode surface. A similar phenomenon was also previously documented [21].

2.2. Ammonia Conversion

The catalytic performances of the Ti_4O_7 electrodes were evaluated using ammonia oxidation as a model reaction. As shown in Figure S5, an evident promotion was observed for ammonia conversion in the flow-through system, with effluent ammonia concentration decreased from 30 to 0.7 $mg{\cdot}L^{-1}$. However, for batch and single-pass systems, the ammonia concentration decreased to 15.1 $mg{\cdot}L^{-1}$ and 26.3 $mg{\cdot}L^{-1}$, respectively, under similar conditions. The improved performance in the flow-through mode can be due to the convection-enhanced mass transport. The removal kinetics was the lowest in single-pass filtration mode, because the liquid residence time within the filtration device was rather limited (5 sec), which caused insufficient contact between ammonia molecules and the electrode. Additionally, in the batch mode, the mass transport of ammonia was only dominated by diffusion and, consequently, only the surface active sites contributed to the ammonia conversion. This demonstrates the advantage of a flow-through design compared to the flow-by mode in conventional batch system.

2.3. Impacts of Key Operational Parameters

2.3.1. Effect of Anode Potential

To study the effect of the anode potential on ammonia oxidation, different anode potentials were exerted. As displayed in Figure 1a, when the anode potential increased from 1.9 V to 2.8 V vs. Ag/AgCl, the ammonia conversion efficiency increased from 43.2% to 85.9%. This indicates that a higher potential was beneficial for ammonia conversion. However, further increasing the anode potential to 3.1 V vs. Ag/AgCl contributed negatively to the ammonia oxidation kinetics, due to the occurrence of other side reactions, such as oxygen evolution reaction, which decreased the overall current efficiency [22]. Hence, 2.8 V vs. Ag/AgCl was selected as optimal for subsequent studies.

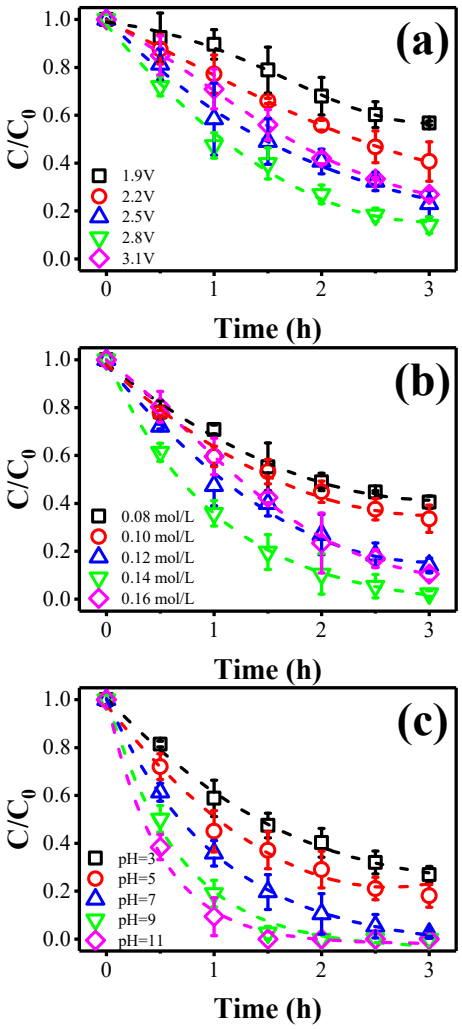

Figure 1. The effect of different operational factors on the ammonia removal: impact of (**a**) anode potential, (**b**) [Cl^-] concentration, and (**c**) solution pH.

2.3.2. Effect of [Cl^-]

As shown in Figure 1b, when the [Cl^-] concentration increased from 0.08 M to 0.14 M, the ammonia conversion increases sharply from 59.6% to 97.8%. This may be due to the increase of chloride ions producing more radicals (e.g., Cl• and ClO•) and contributing to the radical-mediated ammonia oxidation reaction [22]. However, further increasing [Cl^-] concentration to 0.16 M caused a slight decrease in the ammonia oxidation efficiency. Other side reactions may occur in the presence of excess [Cl^-] (Equations (1) and (2)), which consumes as-produced radicals and, hence, reduces the overall ammonia conversion efficiency [22].

$$Cl\bullet + Cl^- \rightarrow Cl_2^{\bullet -} \quad (1)$$

$$Cl_2^{\bullet -} + H_2O \rightarrow HOCl + Cl^- + H^+ + e^- \quad (2)$$

2.3.3. Effect of Solution pH

The effect of initial solution pH on the ammonia removal was studied and the results are displayed in Figure 1c. The removal efficiency of ammonia after 3 h was 73.2% at pH 3 and 81.9% at pH 5. This may be attributed to the poor stability of hypochlorous acid under acidic conditions [23]. However, the conversion efficiency of ammonia significantly improved under alkaline conditions. At pH 9 and 11, the ammonia conversion rate after 1.5 h was 97.4% and 100%, respectively. Ammonia in the aqueous solution may be present in the non-ionized form (NH_3) or the ionized form (NH_4^+)

(Equation (3)) [24]. In these two forms, the non-ionized ammonia is more susceptible to oxidation [25]. According to Candido et al., NH_3 is the dominant species in alkaline media, with a pH greater than 10. When pH < 7, NH_4^+ is a dominant species. In the medium pH, the two substances are in equilibrium [26]. Besides, alkaline conditions also promoted the cycling of Cl^- and enhanced indirect oxidation [23]. Considering the ammonia loss caused by stripping ammonia in the solution under the pH of 11 [27], we chose pH 9 for subsequent investigations.

$$Cl_2^{\bullet -} + H_2O \rightarrow HOCl + Cl^- + H^+ + e^- \quad (3)$$

2.3.4. Effect of Flow Rate

The effect of flow rate on the ammonia oxidation is available in Figure S6. When the flow rate increased from 0.5 to 1.5 mL·min^{-1}, the ammonia conversion efficiency increased from 73.7% to 97.4%. However, further increasing flow rate to 2.0 mL·min^{-1} caused a slight decrease in ammonia oxidation performance. This can be explained by the fact that a higher flow rate may shorten the residence time within the filtration system and cause incomplete ammonia reaction.

2.4. Ammonia Decontamination Mechanism

EPR and radical quenching experiments were carried out to identify the main active substances for ammonia conversion. As shown in Figure 2a, the signal of DMPO–ClO• was detected in the presence of [Cl^-] [28,29]. A four-line characteristic DMPO−OH• signal with 1:2:2:1 intensity was observed, and other faint peaks may correspond to Cl• [30]. Similar results were previously reported by Zhang et al. [29]. This confirmed the generation of ClO•, OH• and Cl• within the present electrochemical flow-through system. Furthermore, radical quenching tests were performed using nitrobenzene (NB), tert-butanol (tBuOH), and HCO_3^- as scavengers (Figure 2b). NB reacts rapidly with OH•, while tBuOH has high affinity to HO•, Cl•, and ClO• [22,31]. In addition, HCO_3^- can be served as a scavenger for HO• and Cl•, while its reaction with ClO• is negligible [32]. In comparison with the control experiments, free of any scavengers, tBuOH showed complete inhibition to the conversion of ammonia, indicating the importance of radicals in ammonia conversion. In contrast, the efficiency of ammonia conversion was only reduced by 15% after the introduction of NB, implying that OH• was not the major radical. We also found that the addition of $NaHCO_3$ did not completely inhibit the conversion of ammonia, suggesting that ClO• was the main oxidant. In addition, we conducted another control experiment using Na_2SO_4 instead of NaCl. As expected, only the DMPO−OH• signal (Figure 2a) and negligible ammonia conversion (< 8%) were observed (Figure S7), further verifying the essential role of [Cl^-].

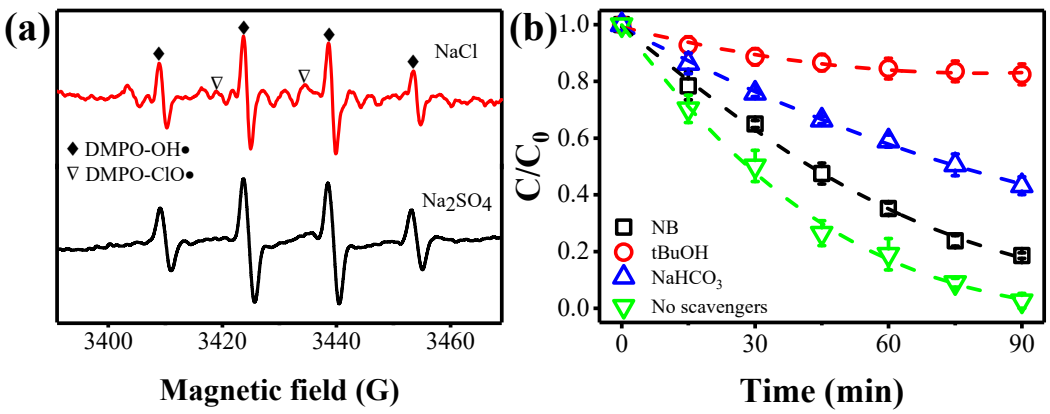

Figure 2. (**a**) EPR spectra with DMPO observed from the flow-through experiment. (**b**) Effect of different scavengers on ammonia removal.

Based on the above discussion, a plausible mechanism of ammonia conversion was proposed and illustrated in Figure 3. On the surface of the Ti_4O_7 anode, water and chloride ions were effectively oxidized under high potential (e.g., 2.8 V vs. Ag/AgCl) to generate OH• and free chlorine (e.g., HClO or ClO^-), respectively. The ClO• can be produced by the instantaneous adduct of OH• with free chlorine (Equations (4) and (5)) [33,34]. In particular, the ClO• can react selectively with NH_4^+ ($k_{ClO•}$ = 3.1 × 10^9 M^{-1} s^{-1}), compared with that of OH• ($k_{OH•}$ = 8.9 × 10^7 M^{-1} s^{-1}) and Cl• ($k_{Cl•}$ = 1.1 × 10^9 M^{-1} s^{-1}) [29].

$$OH• + HClO \rightarrow ClO• + H_2O \quad (4)$$

$$OH• + OCl^- \rightarrow ClO• + OH^- \quad (5)$$

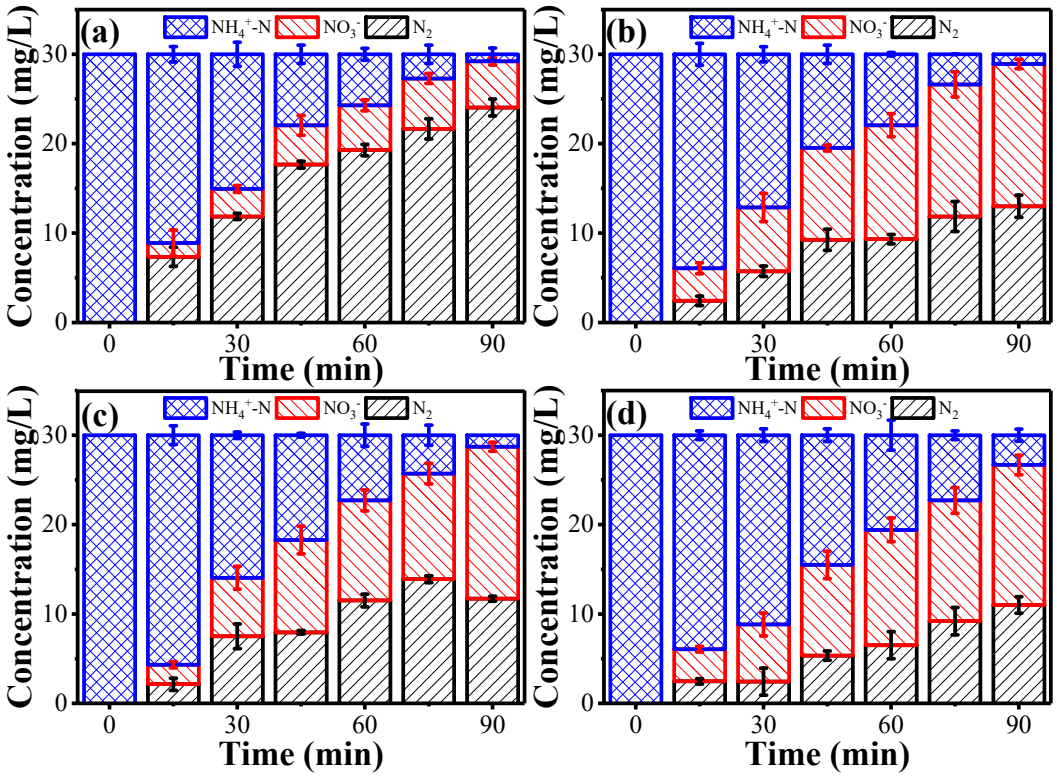

Figure 3. The conversion of ammonia in 90 min by employing different cathode materials: (**a**) Pd-Cu/NF, (**b**) Pd/NF, (**c**) Cu/NF, and (**d**) NF. Reaction conditions: anode potential of 2.8 V vs. Ag/AgCl, [Cl^-] of 0.14 M, flow rate of 1.5 mL·min^{-1}, and pH 9.

These ClO• radicals would extract H from the NH_4^+ molecules to form the N-centered radicals (e.g., •NHCl) [34], while the N-centered radicals would be unstable [29]. Once formed, these •NHCl would undergo self-decay to produce N_2 (Equations (6)–(8)) [35]. In addition, NO_3^- may be produced during this process, resulting in incomplete denitrification (Equations (9) and (10)).

$$NH_4^+ + ClO• \rightarrow NH_2Cl + OH• + H^+ \quad (6)$$

$$NH_2Cl + ClO• \rightarrow •NHCl + HClO \quad (7)$$

$$•NHCl \xrightarrow{•NHCl} N_2 + 2H^+ + 2Cl^- \quad (8)$$

$$NH_4^+ + 8Cl• + 3H_2O \rightarrow NO_3^- + 8Cl^- + 10H^+ \quad (9)$$

$$NH_4^+ + 4HClO \rightarrow NO_3^- + H_2O + 6H^+ + 4Cl^- \quad (10)$$

2.5. Nitrate Reduction on the Pd-Cu/NF Cathode

NO_3^- was difficult to attach onto the cathode surface, due to the like-charge repulsion by the negatively-charged cathode. Moreover, these NO_3^- can be converted back to NH_4^+ as well. To alleviate this issue, a Pd-Cu/NF, with three-dimensional network and excellent electrical conductivity, was used as the cathode material [2,36,37]. It is of note that the coating of Pd and Cu is indispensable. These adsorbed NO_3^- anions were reduced to NO_2^- at the Cu sites and further reduced to N_2 at the Pd sites of the cathode [30]. Results suggest that a similar ammonia removal kinetics was observed using a Cu-NF or a Pd-NF cathode, and the NO_3^- generated was 15.9 and 17.1 mg·L^{-1}, respectively. However, the integration of Pd-Cu sites evidently boosted the kinetics of NO_3^- reduction to N_2 and inhibited the conversion of NH_4^+ to NO_3^-, resulting in only 5.1 mg·L^{-1} NO_3^-, while the presence of Pd or Cu-alone only led to limited N_2 yield (Figure 3). For the NF cathode, the ammonia conversion rate was rather slower, while the NO_3^- reduction rate is similar to the Pd/NF or the Cu/NF cathode.

2.6. Stability Evaluation of the Ti_4O_7 Electrode

The stability of the anode is important for practical applications. Hence, the stability of the Ti_4O_7 electrode was evaluated in consecutive cycles for ammonia conversion under the conditions of potential 2.8 V vs. Ag/AgCl, [Cl^-] of 0.14 M, and pH 9. Figure 4a shows that only marginal declines in ammonia removal efficiency were experienced in the three cycles, indicating the outstanding stability of the Ti_4O_7 electrode in catalytic oxidation. In addition, the ammonia conversion was further examined under actual water matrixes. To do this, the 30 mg·L^{-1} ammonia-spiked lake water and the tap water were challenged with the filtration system under optimal conditions. Results suggest that a similar ammonia oxidation trend was obtained in tap water samples when compared to that in DI water conditions (Figure 4b). Moreover, a > 91.7% ammonia conversion was achieved when challenging with the ammonia-spiked lake water (TOC = 96.3 mg·L^{-1}), which was considered as a more complex matrix compared to tap or DI water. Moreover, the energy consumption of electrochemical filtration was calculated at a typical total cell potential of 3.6 V (corresponds to a potential of 2.8 V vs. Ag/AgCl) to be 2.31 kWh·kg^{-1} COD for the proposed technology. These values are comparable to or even lower than current state-of-the-art electrochemical oxidation processes, with a power consumption of 5–100 kWh·kg^{-1} COD [5]. In addition, the energy per volume is only 0.4 kWh·m^{-3}, comparable to the most advanced electrochemical processes with energy consumption in the range of 0.1–40 kWh·m^{-3} [38]. This indicates that the electroactive filtration system can be served as a promising unit for ammonia decontamination.

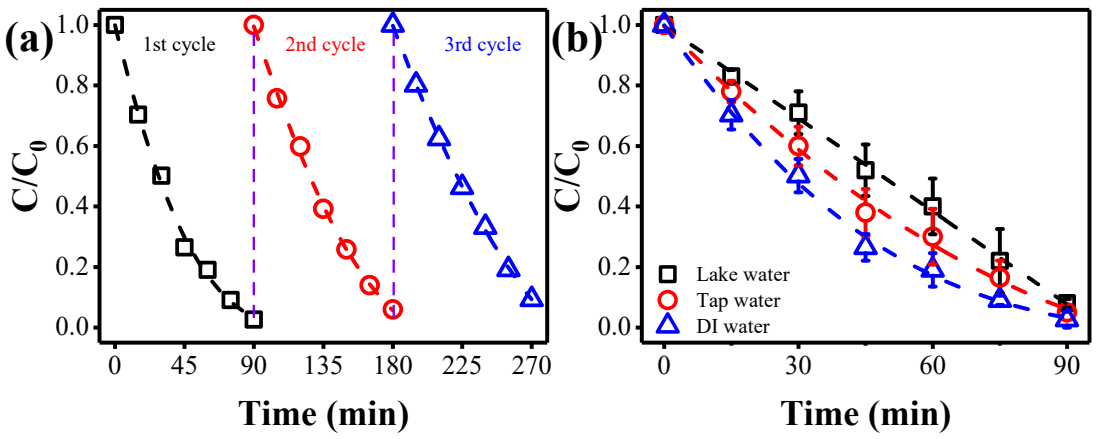

Figure 4. (**a**) Comparison of ammonia conversion kinetics during three consecutive cycles. (**b**) Impact of background solutions on the ammonia removal. Reaction conditions: ammonia of 30 mg·L^{-1}, anode potential of 2.8 V vs. Ag/AgCl, flow rate of 1.5 mL·min^{-1}, [Cl^-] of 0.14 M, and pH 9.

3. Materials and Methods

3.1. Chemicals and Materials

The Ti_4O_7 powder was provided by Kelai New Material Co., Ltd. (Hunan, China). Nickel foam (NF, 0.5 mm thickness) was supplied by Lizhiyuan Electronics Co., Ltd. (Shanxi, China). Sulfuric acid (H_2SO_4, 96%–98%), acetone (≥ 99.5%), hydrochloric acid (HCl, 36%–38%), sodium hydroxide (NaOH, ≥ 96%), copper(II) sulfate pentahydrate ($CuSO_4 \cdot 5H_2O$, ≥ 99%), palladium (II) chloride ($PdCl_2$, ≥ 98%), ammonium sulfate ($(NH_4)_2SO_4$, ≥ 99%), sodium chloride (NaCl, ≥ 99.5%), and sodium sulfate (Na_2SO_4, ≥ 99%) were purchased from Sinopharm Chemical Reagent Co., Ltd. (Shanghai, China).

3.2. Preparation of Electrodes

The Ti_4O_7 anodes were synthesized by mixing 1 g Ti_4O_7 powder with 2–3 wt % paraffin oil as binder. The powder and binder were mixed for 10 min. The mixture was transferred in module (D = 1.2 cm) and a pressure of ~ 50 kg was applied by a hydraulic tablet machine (Lixin experimental instrument, Shenzhen, China). The sheets were sintered in a tube furnace at N_2 atmosphere at 900 °C for 6 h. The fabrication of Pd-Cu/NF, Pd/NF, and Cu/NF electrodes followed a previously reported electrodeposition method [39].

3.3. Electrochemical Experiments

The ammonia degradation experiment was carried out in a customized flow-through electrochemical apparatus (Figure S8), including a Ti_4O_7 working electrode, a Pd-Cu/NF counter electrode, and a saturated Ag/AgCl reference electrode. In a typical experiment, 30 mL of 30 $mg \cdot L^{-1}$ $(NH_4)_2SO_4$ solution and certain NaCl electrolyte were passed through the filtration casing and then returned. The flow rate was tuned by a Cole-Parmer ISM833C peristaltic pump (Vernon Hills, IL, USA). The applied voltage was provided by a Chenhua CHI 760E electrochemical workstation (Shanghai, China). Solution pH was adjusted by 0.1 M H_2SO_4 or NaOH. Ammonia concentration in the influent and effluent was measured by the standard Nessler reagent method. NO_3^- and NO_2^- concentration was determined by a Thermo Fisher DionexTM ICS-5000 ion chromatography (IC, Waltham, MA, USA).

3.4. Analytical Methods

A Hitachi S-4800 field emission scanning electron microscope (FESEM, Tokyo, Japan) and a Rigaku D/max-2550/PC X-ray diffraction (XRD, Austin, TX, USA) was applied to characterize surface morphologies and crystal phases of the electrode materials, respectively. X-ray photoelectron spectroscopy (XPS, Model No.: Thermo Fisher Scientific Escalab 250Xi, Waltham, MA, USA) was performed under high vacuum. Total organic carbon (TOC) was measured by a multi N/C 2100 TOC Analyzer (Analytik Jena AG, City, Germany). A MS5000 electron paramagnetic resonance (EPR) spectrometer (Freiberg Instruments Inc., Freiberg, Germany) was employed to examine produced reactive radicals. The Brunauer Emmett Teller (BET) surface area of the electrode materials was performed using an Anton Paar Autosorb iQ-c analyzer (Boynton Beach, FL, USA).

4. Conclusions

This work presents an effective design of a continuous-flow electrochemical system towards selective and efficient decontamination of ammonia from water. The proposed technology consists of a Ti_4O_7-based anode and a Pd-Cu/NF cathode; both are indispensable. Upon the application of an external electric field, the system enables a sustainable production of ClO•, which then reacts with ammonia selectively to produce N_2. Any anodic byproducts were further reduced to N_2 again at the cathode. Various advanced characterizations were employed to confirm the effectiveness of the

system. This study extends the application of electrocatalytic technology and provides an affordable and feasible strategy for water remediation.

Supplementary Materials: The following are available online at http://www.mdpi.com/2073-4344/10/4/383/s1, Figure S1: (**a**) FESEM characterization, (**b**) XRD pattern, and (**c**) XPS survey pattern of the Ti_4O_7 anode. XPS narrow scan of (**d**) Ti 2p on Ti_4O_7 electrode; Figure S2. XPS spectra for the narrow scan of (**a**) C 1s, and (**b**) O 1s on Ti_4O_7 electrode; Figure S3: Digital pictures of (**a**) Pd-Cu/NF electrode, (**b**) Pd/NF electrode, (**c**) Cu/NF electrode, and (**d**) pure Ni foam electrode; Figure S4: FESEM images (**a**, **b**) of the Pd/Cu-Ni foam electrode. XPS spectra for the narrow scan of (**c**) Pd and (**d**) Cu of a fresh Pd-Cu/NF cathode; Figure S5: Comparison of ammonia conversion kinetics in batch, single-pass, and flow-through systems; Figure S6. The effect of flow rate on ammonia conversion. Reaction conditions: anode potential of 2.8 V vs. Ag/AgCl, [Cl^-] concentration of 0.14 M, and pH of 9; Figure S7: Conversion effect of ammonia with 0.14 M Na_2SO_4 background electrolyte at different anode potentials; Figure S8. Schematic of the flow-through filtration setup. (**a**) Modified acrylic filter sleeve, including (1) a Ti_4O_7 anode, (2) a Ti plate current collector, and (3) a Pd-Cu/NF cathode. (**b**, **d**) Images of the modified filter sleeve. (**c**, **e**) Images of the anode and cathode; Table S1. Comparison of the performance of different materials on ammonia conversion.

Author Contributions: Data curation, writing—original draft preparation, W.Z. and J.M.; conceptualization, supervision, funding acquisition, Y.L. and B.Y.; investigation, methodology, F.L., Y.L., and X.F.; formal analysis, resources, M.H. and W.Z.; writing—review and editing, W.Z., Y.L., and W.S. All authors have read and agreed to the published version of the manuscript.

Funding: This research was funded by the Natural Science Foundation of Shanghai, China (No. 18ZR1401000), and the Shanghai Pujiang Program (No. 18PJ1400400).

Conflicts of Interest: The authors declare no conflicts of interest.

References

1. Weihrauch, D.; Donini, A.; O'Donnell, M.J. Ammonia transport by terrestrial and aquatic insects. *J. Insect Physiol.* **2012**, *58*, 473–487. [CrossRef]
2. Zhang, C.Y.; He, D.; Ma, J.X.; Waite, T.D. Active chlorine mediated ammonia oxidation revisited: Reaction mechanism, kinetic modelling and implications. *Water Res.* **2018**, *145*, 220–230. [CrossRef]
3. Gayen, P.; Chen, C.; Abiade, J.T.; Chaplin, B.P. Electrochemical oxidation of atrazine and clothianidin on Bi-doped SnO_2-Ti_nO_{2n-1} electrocatalytic reactive electrochemical membranes. *Environ. Sci. Technol.* **2018**, *52*, 12675–12684. [CrossRef]
4. Li, M.H.; Liu, Y.B.; Dong, L.M.; Shen, C.S.; Li, F.; Huang, M.H.; Ma, C.Y.; Yang, B.; An, X.Q.; Sand, W. Recent advances on photocatalytic fuel cell for environmental applications-The marriage of photocatalysis and fuel cells. *Sci. Total Environ.* **2019**, *668*, 966–978. [CrossRef]
5. Chaplin, B.P. The prospect of electrochemical technologies advancing worldwide water treatment. *Acc. Chem. Res.* **2019**, *52*, 596–604. [CrossRef]
6. Li, F.; Peng, X.; Liu, Y.B.; Mei, J.C.; Sun, L.W.; Shen, C.S.; Ma, C.Y.; Huang, M.H.; Wang, Z.W.; Sand, W.G. A chloride-radical-mediated electrochemical filtration system for rapid and effective transformation of ammonia to nitrogen. *Chemosphere* **2019**, *229*, 383–391. [CrossRef]
7. Liu, Y.B.; Wu, P.; Liu, F.Q.; Li, F.; An, X.Q.; Liu, J.S.; Wang, Z.W.; Shen, C.S.; Sand, W. Electroactive modified carbon nanotube filter for simultaneous detoxification and sequestration of Sb(III). *Environ. Sci. Technol.* **2019**, *53*, 1527–1535. [CrossRef]
8. Zaky, A.M.; Chaplin, B.P. Porous substoichiometric TiO_2 anodes as reactive electrochemical membranes for water treatment. *Environ. Sci. Technol.* **2013**, *47*, 6554–6563. [CrossRef]
9. Le, T.X.H.; Haflich, H.; Shah, A.D.; Chaplin, B.P. Energy-efficient electrochemical oxidation of perfluoroalkyl substances using a Ti_4O_7 reactive electrochemical membrane anode. *Environ. Sci. Technol. Lett.* **2019**, *6*, 504–510. [CrossRef]
10. Chaplin, B.P. Critical review of electrochemical advanced oxidation processes for water treatment applications. *Environ. Sci. Process. Impacts* **2014**, *16*, 1182–1203. [CrossRef]
11. Donaghue, A.; Chaplin, B.P. Effect of select organic compounds on perchlorate formation at boron-doped diamond film anodes. *Environ. Sci. Technol.* **2013**, *47*, 12391–12399. [CrossRef]
12. Liu, Y.B.; Mei, J.C.; Shen, C.S.; Huang, M.H.; Yang, M.; Wang, Z.W.; Sand, W.; Li, F. Rapid and selective electrochemical transformation of ammonia to N_2 by substoichiometric TiO_2-based electrochemical system. *RSC Adv.* **2020**, *10*, 1219–1225. [CrossRef]

13. Kong, X.J.; Wu, Z.H.; Ren, Z.R.; Guo, K.H.; Hou, S.D.; Hua, Z.C.; Li, X.C.; Fang, J.Y. Degradation of lipid regulators by the UV/chlorine process: Radical mechanisms, chlorine oxide radical (ClO•)-mediated transformation pathways and toxicity changes. *Water Res.* **2018**, *137*, 242–250. [CrossRef]
14. Nayak, S.; Chaplin, B.P. Fabrication and characterization of porous, conductive, monolithic Ti_4O_7 electrodes. *Electrochim. Acta* **2018**, *263*, 299–310. [CrossRef]
15. Liang, S.T.; Lin, H.; Yan, X.F.; Huang, Q.G. Electro-oxidation of tetracycline by a Magneli phase Ti_4O_7 porous anode: Kinetics, products, and toxicity. *Chem. Eng. J.* **2018**, *332*, 628–636. [CrossRef]
16. Tao, X.Y.; Wang, J.G.; Ying, Z.G.; Cai, Q.X.; Zheng, G.Y.; Gan, Y.P.; Huang, H.; Xia, Y.; Liang, C.; Zhang, W.K.; et al. Strong sulfur binding with conducting Magneli-phase Ti_nO_{2n-1} nanomaterials for improving lithium-sulfur batteries. *Nano Lett.* **2014**, *14*, 5288–5294. [CrossRef]
17. Boffa, A.B.; Galloway, H.C.; Jacobs, P.W.; Benitez, J.J.; Batteas, J.D.; Salmeron, M.; Bell, A.T.; Somorjai, G.A. The growth and structure of titanium oxide films on Pt(111) investIgated by LEED, XPS, ISS, and STM. *Surf. Sci.* **1995**, *326*, 80–92. [CrossRef]
18. Jiang, X.H.; Xing, Q.J.; Luo, X.B.; Li, F.; Zou, J.P.; Liu, S.S.; Li, X.; Wang, X.K. Simultaneous photoreduction of Uranium(VI) and photooxidation of Arsenic (III) in aqueous solution over g-C_3N_4/TiO_2 heterostructured catalysts under simulated sunlight irradiation. *Appl. Catal. B-Environ.* **2018**, *228*, 29–38. [CrossRef]
19. Zeng, H.B.; Liu, S.S.; Chai, B.Y.; Cao, D.; Wang, Y.; Zhao, X. Enhanced photoelectrocatalytic decomplexation of Cu-EDTA and Cu recovery by persulfate activated by UV and cathodic reduction. *Environ. Sci. Technol.* **2016**, *50*, 6459–6466. [CrossRef]
20. Liu, C.; Hirohara, M.; Maekawa, T.; Chang, R.; Hayashi, T.; Chiang, C.Y. Selective electro-oxidation of glycerol to dihydroxyacetone by a non-precious electrocatalyst-CuO. *Appl. Catal. B.-Environ.* **2020**, *265*, 12. [CrossRef]
21. Yuan, H.K.; Kusema, B.T.; Yan, Z.; Streiff, S.; Shi, F. Highly selective synthesis of 2,5-bis(aminomethyl)furan via catalytic amination of 5-(hydroxymethyl)furfural with NH_3 over a bifunctional catalyst. *RSC Adv.* **2019**, *9*, 38877–38881. [CrossRef]
22. Ji, Y.Z.; Bai, J.; Li, J.H.; Luo, T.; Qiao, L.; Zeng, Q.Y.; Zhou, B.X. Highly selective transformation of ammonia nitrogen to N_2 based on a novel solar-driven photoelectrocatalytic-chlorine radical reactions system. *Water Res.* **2017**, *125*, 512–519. [CrossRef]
23. Deng, Y.; Englehardt, J.D. Electrochemical oxidation for landfill leachate treatment. *Waste Manag.* **2007**, *27*, 380–388. [CrossRef]
24. Kim, K.W.; Kim, Y.J.; Kim, I.T.; Park, G.I.; Lee, E.H. The electrolytic decomposition mechanism of ammonia to nitrogen at an IrO_2 anode. *Electrochim. Acta* **2005**, *50*, 4356–4364. [CrossRef]
25. Bunce, N.J.; Bejan, D. Mechanism of electrochemical oxidation of ammonia. *Electrochim. Acta* **2011**, *56*, 8085–8093. [CrossRef]
26. Candido, L.; Gomes, J. Evaluation of anode materials for the electro-oxidation of ammonia and ammonium ions. *Mater. Chem. Phys.* **2011**, *129*, 1146–1151. [CrossRef]
27. Kim, K.W.; Kim, Y.J.; Kim, I.T.; Park, G.I.; Lee, E.H. Electrochemical conversion characteristics of ammonia to nitrogen. *Water Res.* **2006**, *40*, 1431–1441. [CrossRef]
28. Hao, R.L.; Mao, X.Z.; Wang, Z.; Zhao, Y.; Wang, T.H.; Sun, Z.H.; Yuan, B.; Li, Y.K. A novel method of ultraviolet/$NaClO_2$-NH_4OH for NO removal: Mechanism and kinetics. *J. Hazard. Mater.* **2019**, *368*, 234–242. [CrossRef]
29. Zhang, Y.; Li, J.H.; Bai, J.; Li, L.S.; Chen, S.; Zhou, T.S.; Wang, J.C.; Xia, L.G.; Xu, Q.J.; Zhou, B.X. Extremely efficient decomposition of ammonia N to N_2 using ClO• from reactions of HO• and HOCl generated in situ on a novel bifacial photoelectroanode. *Environ. Sci. Technol.* **2019**, *53*, 6945–6953. [CrossRef]
30. Tang, W.J.; Zhang, Y.; Bai, J.; Li, J.H.; Wang, J.C.; Li, L.S.; Zhou, T.S.; Chen, S.; Rahim, M.; Zhou, B.X. Efficient denitrification and removal of natural organic matter, emerging pollutants simultaneously for RO concentrate based on photoelectrocatalytic radical reaction. *Sep. Purif. Technol.* **2020**, *234*, 116032. [CrossRef]
31. Cheng, X.W.; Liu, H.L.; Chen, Q.H.; Li, J.J.; Wang, P. Preparation and characterization of palladium nano-crystallite decorated TiO_2 nano-tubes photoelectrode and its enhanced photocatalytic efficiency for degradation of diclofenac. *J. Hazard. Mater.* **2013**, *254*, 141–148. [CrossRef] [PubMed]
32. Guo, K.H.; Wu, Z.H.; Shang, C.; Yao, B.; Hou, S.D.; Yang, X.; Song, W.H.; Fang, J.Y. Radical chemistry and structural relationships of PPCP degradation by UV/chlorine treatment in simulated drinking water. *Environ. Sci. Technol.* **2017**, *51*, 10431–10439. [CrossRef]

33. Hua, Z.C.; Guo, K.H.; Kong, X.J.; Lin, S.K.; Wu, Z.H.; Wang, L.P.; Huang, H.; Fang, J.Y. PPCP degradation and DBP formation in the solar/free chlorine system: Effects of pH and dissolved oxygen. *Water Res.* **2019**, *150*, 77–85. [CrossRef] [PubMed]
34. Wu, Z.H.; Guo, K.H.; Fang, J.Y.; Yang, X.Q.; Xiao, H.; Hou, S.D.; Kong, X.J.; Shang, C.; Yang, X.; Meng, F.A.; et al. Factors affecting the roles of reactive species in the degradation of micropollutants by the UV/chlorine process. *Water Res.* **2017**, *126*, 351–360. [CrossRef]
35. De Laat, J.; Boudiaf, N.; Dossier-Berne, F. Effect of dissolved oxygen on the photodecomposition of monochloramine and dichloramine in aqueous solution by UV irradiation at 253.7 nm. *Water Res.* **2010**, *44*, 3261–3269. [CrossRef] [PubMed]
36. Yoshinaga, Y.; Akita, T.; Mikami, I.; Okuhara, T. Hydrogenation of nitrate in water to nitrogen over Pd-Cu supported on active carbon. *J. Catal.* **2002**, *207*, 37–45. [CrossRef]
37. Gao, W.L.; Guan, N.J.; Chen, J.X.; Guan, X.X.; Jin, R.C.; Zeng, H.S.; Liu, Z.G.; Zhang, F.X. Titania supported Pd-Cu bimetallic catalyst for the reduction of nitrate in drinking water. *Appl. Catal. B-Environ.* **2003**, *46*, 341–351. [CrossRef]
38. Panizza, M.; Cerisola, G. Direct and mediated anodic oxidation of organic pollutants. *Chem. Rev.* **2009**, *109*, 6541–6569. [CrossRef]
39. Zhang, Y.; Li, J.H.; Bai, J.; Shen, Z.X.; Li, L.S.; Xia, L.G.; Chen, S.; Zhou, B.X. Exhaustive conversion of inorganic nitrogen to nitrogen gas based on a photoelectro-chlorine cycle reaction and a highly selective nitrogen gas generation cathode. *Environ. Sci. Technol.* **2018**, *52*, 1413–1420. [CrossRef]